





Constraints on the proton fraction of cosmic rays at the highest energies and the consequences for cosmogenic neutrinos and photons

Domenik Ehlert ^{1,2}★ Arjen van Vliet ^{3,2} Foteini Oikonomou ¹ Walter Winter ²

¹Norwegian University of Science and Technology (NTNU), NO-7491 Trondheim, Norway

²Deutsches Elektronen-Synchrotron (DESY), Platanenallee 6, DE-15738 Zeuthen, Germany

³Department of Physics, Khalifa University, P.O. Box 127788, Abu Dhabi, United Arab Emirates

Accepted XXX. Received YYY; in original form ZZZ

ABSTRACT

Over the last decade, observations have shown that the mean mass of ultra-high-energy cosmic rays (UHECRs) increases progressively toward the highest energies. However, the precise composition is still unknown, and several theoretical studies hint at the existence of a subdominant proton component up to the highest energies. Motivated by the exciting prospect of performing charged-particle astronomy with ultra-high-energy (UHE) protons we quantify the level of UHE-proton flux that is compatible with present multimessenger observations and the associated fluxes of neutral messengers produced in the interactions of the protons. We study this scenario with numerical simulations of two independent populations of extragalactic sources and perform a fit to the combined UHECR energy spectrum and composition observables, constrained by diffuse gamma-ray and neutrino observations. We find that up to of order 10% of the cosmic rays at the highest energies can be UHE protons, although the result depends critically on the selected hadronic interaction model for the air showers. Depending on the maximum proton energy ($E_{\text{max}}^{\text{p}}$) and the redshift evolution of sources, the associated flux of cosmogenic neutrinos and UHE gamma rays can significantly exceed the multimessenger signal of the mixed-mass cosmic rays. Moreover, if $E_{\text{max}}^{\text{p}}$ is above the GZK limit, we predict a large flux of UHE neutrinos above EeV energies that is absent in alternate scenarios for the origin of UHECRs. We present the implications and opportunities afforded by these UHE proton, neutrino and photon fluxes for future multimessenger observations.

Key words: astroparticle physics — cosmic rays — neutrinos — gamma-rays — methods:numerical

1 INTRODUCTION

Ultra-high-energy cosmic rays (UHECRs), charged particles of astrophysical origin with energy above $\sim 10^{18}$ eV, are the most energetic cosmic messengers and are, as such, probes of the most extreme astrophysical environments. Because of extragalactic and Galactic magnetic fields, their sources remain elusive, even after years of high-precision observation by the latest generation of UHECR detectors, in particular the Pierre Auger Observatory (Auger) and the Telescope Array (TA).

Observations suggest that the composition of UHECRs is surprisingly pure, with each accelerated nuclear species only dominant in a very narrow band of the UHECR spectrum, and the entire spectrum is produced through a carefully-tuned combination of the individual peaks (e.g. Unger et al. 2015; Aab et al. 2017b; Alves Batista et al. 2019; Heinze et al. 2019). The combination of a smooth increase of average mass and pure composition at all energies implies that the population variance of sources must be remarkably low (Ehlert et al. 2022; see also Heinze et al. 2020). Under these circumstances, the observed flux-cut-off at $E_{\text{CR}} \gtrsim 50$ EeV is generally predicted to be an effect of the maximum particle energy reachable at the cosmic accelerators. Within this “Peters cycle” (Peters 1961; Gaisser et al. 2016)

model of cosmic-ray acceleration with rigidity-dependent maximum energy, no light cosmic rays (CRs) are expected at the highest energies.

Nevertheless, the existence of protons or light nuclei at the highest energies, where there are no measurements of composition-sensitive observables with the fluorescence detectors of Auger and TA, cannot be ruled out at present. A very interesting possibility would be the existence of an additional proton-dominated component at the highest energies. Such a flux cannot be easily explained by reprocessing of accelerated UHECR within the source as proposed for extragalactic protons below the ankle, see e.g. Unger et al. (2015), but must originate from a secondary population of independent sources that exclusively accelerates protons to ultra-high energies or where heavier nuclei are efficiently disintegrated before escaping the source region. Motivations for an additional source population come from the expected differences between possible UHECR accelerators, e.g. active galactic nuclei (Rodrigues et al. 2021) or gamma-ray bursts (Waxman 1995). Such a proton flux does not need to be produced by astrophysical processes necessarily, but could also originate from the decay of heavy dark matter (e.g. Ishiwata et al. (2020); Das et al. (2023)).

Circumstantial evidence for an additional proton component is provided by an apparent flattening of the increase in observed UHECR mass at $E_{\text{CR}} \gtrsim 30$ EeV, as reported in an analysis of Auger surface detector data (Aab et al. 2017d; Todero Peixoto 2019). This feature

★ domenik.ehlert@ntnu.no

could indicate a flux of UHE protons with different spectral index to the bulk of the UHECRs, either from a secondary source population or from a single nearby source (Plotko et al. 2022), but it could also originate from a natural mass limit of the mixed UHECR flux.

Similar two-component models were studied previously, either in the context of the transition region between Galactic and extragalactic cosmic rays below $10^{18.7}$ eV (Mollerach & Roulet 2020; Abreu et al. 2021; Luce et al. 2022; Abdul Halim et al. 2022), or similar to the present paper at the highest energies (Muzio et al. 2019; Das et al. 2021; Muzio et al. 2023). We discuss our findings in the context of existing results in Sec. 6.

UHE protons, should they exist, are of significant interest for “UHECR astronomy” due to their high rigidity and consequently weak deflections in magnetic fields. Additionally, if they are accelerated to energies beyond $\sim 10^{19.7}$ eV, the cross-section for photo-pion production on CMB photons is enhanced due to the Δ -resonance. This effect, known as the Greisen-Zatsepin-Kuzmin (GZK) limit (Greisen 1966; Zatsepin & Kuzmin 1966), leads to strong attenuation of UHE protons above this energy if they are produced in sources more distant than ~ 100 Mpc (see e.g. Gaisser et al. 2016) and the abundant production of charged and neutral pions. The subsequent decay of these pions will result in a large flux of high-energy neutrinos and gamma rays.

In this paper we quantify the maximum flux of UHE protons compatible with current observations of UHECR spectrum and composition, considering multimessenger constraints from gamma rays and neutrinos. We investigate two separate scenarios for the maximum proton energy; (i) a high- $E_{\text{max}}^{\text{p}}$ and (ii) a low- $E_{\text{max}}^{\text{p}}$ scenario.

A brief overview of the model is provided in Sec. 2. Injection and propagation of the cosmic rays are simulated with the Monte-Carlo framework CRPROP 3 (Alves Batista et al. 2016, 2022), taking into account the interaction with the cosmic microwave background and extragalactic background light (Gilmore et al. 2012). The best-fit source parameters are obtained in Sec. 3 by comparing the model predictions with existing observations, and in Sec. 4 we discuss the expected multimessenger signal. A specific, exotic scenario with flux recovery beyond the GZK cutoff is presented in Sec. 5. Finally, we discuss our results in the context of similar existing studies in Sec. 6, and conclude in Sec. 7 that current UHECR data is compatible with a significant contribution by this additional proton component of up to 15% at 20 EeV. The precise value depends critically on the choice of the hadronic interaction model for air shower modelling and the maximum proton energy.

2 METHODS

The primary, **mixed-composition, UHECR sources (MIX)** are modelled following the effective parametrisation introduced in Aab et al. (2017c) but with minor modifications detailed in Ehlert et al. (2022). We assume the acceleration to be universal in particle rigidity¹, following a “Peters cycle”, with a power-law source spectrum and an exponential cutoff at the highest energies. Sources within the MIX population are assumed as identical and the total emission rate per unit volume is

$$Q_A(E) = Q_A^{E_0} \left(\frac{E}{E_0} \right)^{-\gamma} \exp \left(-\frac{E}{Z E_{\text{max}}^{\text{p}}} \right) \quad (1)$$

¹ The rigidity of a particle is defined as $R = E/Z$ in natural units, where Z is the nuclear charge. It is a measure of the susceptibility to magnetic deflections.

for the five injected elements $A \in \{^1\text{H}, ^4\text{He}, ^{14}\text{N}, ^{28}\text{Si}, ^{56}\text{Fe}\}$. Here $Q_A^{E_0}$ is the local emission rate at a normalisation energy $E_0 \ll E_{\text{max}}^{\text{p}}$ in $\text{erg Mpc}^{-3} \text{ yr}^{-1}$, and γ is the spectral index which is ≈ 2 for diffusive shock acceleration. The source emissivity, i.e. the luminosity density, can be derived from the emission rate as

$$L_0 = \sum_A \int_{E_{\text{min}}}^{\infty} dE \left(E \cdot Q_A^{E_0} \right), \quad (2)$$

where we have chosen $E_{\text{min}} = 10^{17.8}$ eV.

The predicted flux at Earth for an observed nuclear mass A' and energy E' , and for a redshift evolution of the source population emissivity $n(z)$, is

$$\phi(E', A') = \sum_A \int dE \int dz \left| \frac{dt}{dz} \right| n(z) Q_A(E) \cdot \frac{dN_{A'}}{dE' dN_A}(E', E, z). \quad (3)$$

The last term translates the injected spectrum at the sources to the observed spectrum after propagation and is obtained via Monte-Carlo simulations with CRPROP 3. In general, the source redshift evolution $n(z)$ is composed of the evolution of per-source luminosities and the density evolution of the source population. In our analysis, we do not attempt to distinguish the difference between these effects and describe the evolution with a (broken) power law

$$n(z) = \begin{cases} (1+z)^m & \text{for } m \leq 0, \\ (1+z)^m & \text{for } m > 0 \text{ and } z < z_0, \\ (1+z_0)^m & \text{for } m > 0 \text{ and } z_0 < z < z_{\text{max}}, \\ 0 & \text{otherwise,} \end{cases} \quad (4)$$

with $z_0 = 1.5$ and $z_{\text{max}} = 4$ (Van Vliet et al. 2019). Sources at $z \gtrsim 1$ have a negligible impact on the observed UHECR flux because of attenuation effects, but they play an important role for the expected multimessenger signal of co-produced neutrinos and low-energy gamma rays. A more conservative estimate of the cosmogenic neutrino flux is obtained if these high-redshift sources, which cannot be constrained by the cosmic-ray fit, are ignored.

For the additional population of **UHE pure-proton sources (PP)**, we are particularly interested in the predicted flux of cosmogenic neutrinos at $E_\nu \approx 1$ EeV since this corresponds to the peak sensitivity interval of many existing and planned neutrino experiments. If these neutrinos are produced in the interactions of cosmic rays with photon fields, they typically receive $\sim 5\%$ of the primary CR energy (Gaisser et al. 2016), which implies that the relevant energy is $E_{\text{CR}} \approx 20$ EeV. We define this value as the reference energy at which we evaluate the contribution of the PP UHE protons to the observed flux of UHECRs. Properties of the pure-proton sources are described by the independent set of parameters $E_{\text{max}}^{\text{pp}}$, γ^{pp} , m^{pp} , and L_0^{pp} .

The interactions of UHECRs with cosmic background photons lead to the production of secondary photons and neutrinos, with the strength of this “cosmogenic” multimessenger signal depending predominantly on the cosmic-ray composition, injection spectral index and source distance. We compare our model predictions for the UHECR spectrum and composition with publicly available data by Auger (Aab et al. 2020; Yushkov 2020). Since the composition cannot be observed directly, the mean, $\langle X_{\text{max}} \rangle$, and standard deviation, $\sigma(X_{\text{max}})$, of the depth of the air-shower maximum are used as proxy observables, and the conversion is performed with the hadronic interaction models EPOS-LHC (Pierog et al. 2015) and SIBYLL2.3C (Fedyntch et al. 2019).

The best-fit source parameters are determined in a two-step fitting process. We discretise the parameter space in maximum energy/rigidity, spectral index and redshift evolution for both source classes and sample a large number of possible combinations of these parameters. For each of these possible source configurations, we then use the Levenberg-Marquardt algorithm² to find the injection fractions f_A of the MIX sources and emissivities $[L_0, L_0^{\text{PP}}]$ of both source populations that minimise the χ^2 differences between our model predictions for the UHECR spectrum and composition and the Auger data points. If a reasonable fit ($\chi^2 < 250$) is found for a particular combination of source parameters then adjacent points are also evaluated in an iterative process.

Constraints on the source parameters derived from a comparison of the predicted cosmogenic flux of gamma rays and neutrinos with observations and upper limits are taken into account with additional $\Delta\chi^2$ -penalty terms. For observed fluxes, such as the Fermi-LAT IGRB (Ackermann et al. 2015) and parts of the IceCube HESE neutrino flux (Abbasi et al. 2021) we consider a simple one-sided χ^2 penalty that only contributes if the predicted flux exceeds observations. For upper-limit points with a low number of, or zero, events per bin, e.g. the Auger UHE neutrino (Pedreira 2021) and UHE gamma-ray limits (Savina 2021; Abreu et al. 2022) we use the Poisson likelihood χ^2 (Baker & Cousins 1984) but the penalty is only applied if the predicted number of events in a bin exceeds the observed number. The relevant data sets are:

- $\Delta\chi_\nu^2$: IceCube HESE flux (Abbasi et al. 2021), (5)
- Auger UHE neutrino limit (Pedreira 2021),
- $\Delta\chi_\gamma^2$: Fermi-LAT IGRB flux (Ackermann et al. 2015),
- Auger hybrid UHE gamma-ray limit (Savina 2021),
- Auger SD UHE gamma-ray limit (Abreu et al. 2022).

We exclude possible source configurations where the combined multimessenger penalty exceeds the level of two sigma, i.e. when $\Delta\chi_\nu^2 + \Delta\chi_\gamma^2 > 4$. However, in the plots of the cosmogenic neutrino and gamma-ray fluxes we only include the rejections by the respective messenger.

3 FIT WITH AN ADDITIONAL PROTON COMPONENT

We investigate two different scenarios in terms of the proton maximum energy, assuming Epos-LHC as hadronic interaction model. Results for SIBYLL2.3c are shown in Appendix A. In both scenarios, we find the redshift evolution of the PP number density to be unconstrained by cosmic-ray observations alone. Since the PP flux is pure protons, interactions during propagation do not affect the observed composition. However, propagation effects soften the distribution and attenuate the original UHE proton flux. Stronger redshift evolutions require harder injection spectra and higher source emissivity.

3.1 Two-Source-Class Dip Model (2SC-dip)

We are particularly interested in scenarios that produce a large flux of UHE neutrinos and gamma rays. This requires proton energies sufficiently above the GZK limit to enable copious photo-pion production on CMB photons, and we, therefore, choose $E_{\text{max}}^{\text{PP}} = 10^{23}$ eV

for our first scenario. The best-fit properties of both source populations are listed in Tab. 1, 2nd column, and the predicted spectrum and composition at Earth are shown in Fig. 1, left. The preferred maximum rigidity, spectral index and redshift evolution of the mixed-composition source population are compatible with the values obtained for the single-population model within uncertainties, and the additional protons provide a relatively constant contribution of approx. 5–10% between the ankle and the end of the GZK cutoff (Fig. 2, teal band). We find that the overall shape effectively corresponds to the predictions from the classical “proton-dip” explanation of the UHECR flux (Berezinsky & Grigor’eva 1988). While this model is inconsistent with current measurements of the UHECR composition and the high-energy neutrino flux (Heinze et al. 2016), our results show that it can still be relevant if the total proton contribution remains subdominant to the primary, mixed-composition, cosmic-ray flux. We refer to the presented source model as the “dip” or 2SC-dip (two-source-class dip) model.

In the 2SC-dip model, the proton sources are required to exhibit a soft injection spectrum (see Appendix B), which could be a distinguishing feature of this additional source population in the observed flux, provided that reliable event-by-event mass reconstruction becomes available in the future. Softer spectra than suggested by the best fit are disfavoured since the associated sub-ankle flux would exceed observational limits. For hard spectra, $\gamma^{\text{PP}} \lesssim 2$, the additional protons only contribute at energies around the GZK cutoff and the possibilities for improving the fit over the entire energy range are consequently limited. The combination of both effects results in a clearly localised preferred spectral index of the proton sources.

3.2 Two-Source-Class Best-Fit Model (2SC-uhecr)

An alternative scenario is presented by proton sources with energies comparable to the standard, mixed-composition, cosmic-ray sources. For this model, we set $E_{\text{max}}^{\text{PP}} = 10$ EeV. At the best fit (Tab. 1, 3rd column), the improvement over the dip-model is $\Delta\chi^2 \approx -15$ but very hard proton spectra are required (see Appendix B). The predicted PP proton spectrum at Earth exhibits a peak-like shape reminiscent of the individual, peaked, mass groups originating from the mixed composition sources (Fig. 1, right). However, due to the choice of $E_{\text{max}}^{\text{PP}}$, the peak energy is shifted upward by approximately an order of magnitude compared to the mixed-population proton peak. Compared to the 2SC-dip model, the best-fit observed proton fraction at 20 EeV is significantly larger, up to 15%, but the contribution is limited to a small energy interval and becomes negligible below the ankle (Fig. 2, brown band).

While this scenario, the “UHECR best-fit” model (2SC-uhecr), provides a significant improvement in the cosmic-ray fit, it comes at the cost of extremely hard proton injection spectra, and the expected cosmogenic neutrino and UHE gamma-ray signal associated with the protons is reduced due to the sub-GZK maximum proton energies. With the injection spectrum of the additional protons similar to the bulk of the cosmic rays, separation of the two components will be difficult even if event-by-event mass reconstruction were available. However, the predicted existence of two separate proton bumps in the cosmic-ray spectrum is a distinguishing feature of this model.

4 MULTIMESSENGER SIGNAL

In the following, we discuss the predicted multimessenger signal produced through interactions with the CMB and the Extragalactic Background Light during the propagation of the cosmic rays. We

² Implemented in the `curve_fit` routine from the `SciPy.optimize` library.

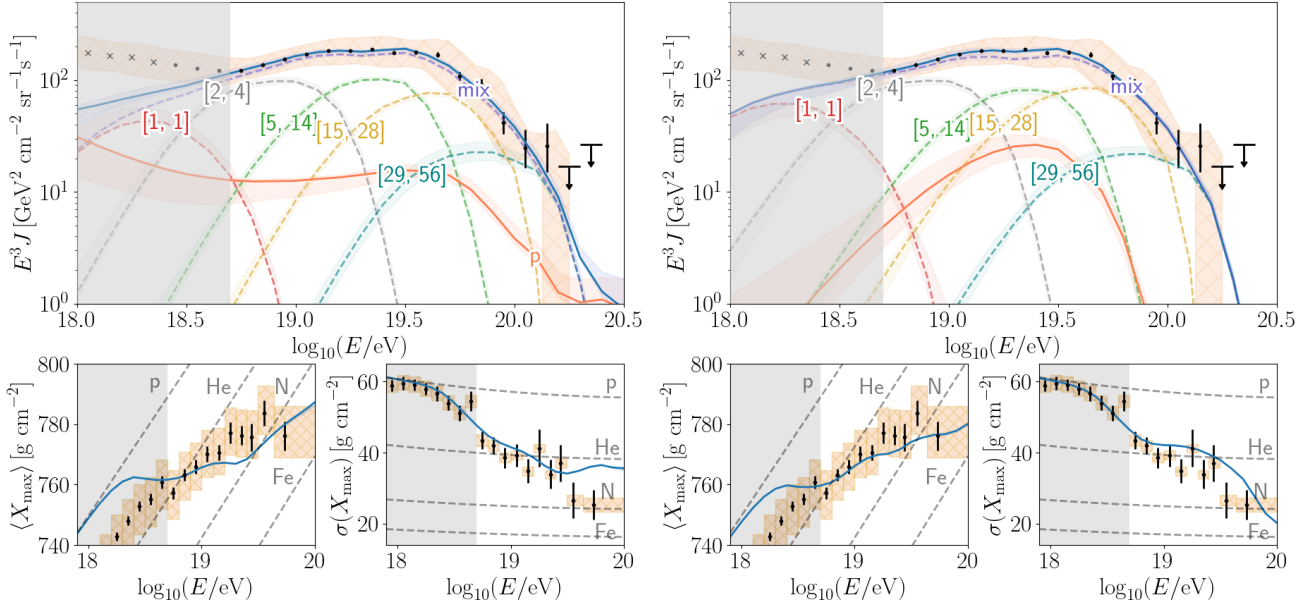


Figure 1. Predicted spectrum and composition at Earth for the three investigated scenarios, with Epos-LHC as hadronic interaction model. Left: “proton-dip” (2SC-dip). Right: “UHECR” best fit (2SC-uhecr). Best-fit parameter values are listed in Tab. 1. Dashed lines indicate the contributions of the separate mass groups from the mixed-composition sources, with $[A_{\min}, A_{\max}]$. The additional protons from the second population are shown as a solid, orange line. Coloured bands indicate the 68% uncertainties.

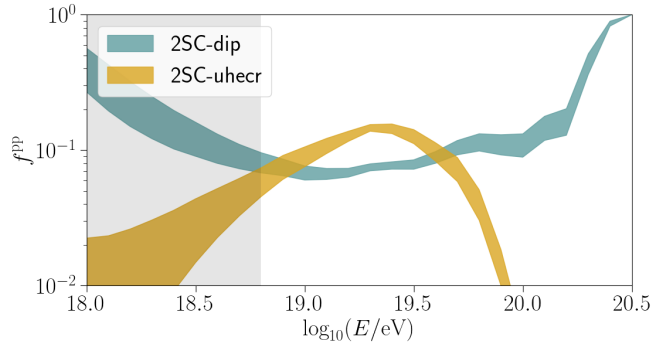


Figure 2. Contribution of the PP protons to the observed, differential UHECR flux as a function of energy, within 1σ of the best fit to CR spectrum and composition (Fig. 1).

focus on the 2SC-dip “proton-dip” model which predicts a large flux of cosmogenic neutrinos and UHE gamma rays. The multimessenger signal of the 2SC-uhecr model is briefly discussed at the end.

4.1 2SC-dip

Photons, electrons, and positrons produced with PeV-EeV energies in photohadronic interactions of the UHE protons interact with cosmic photon fields, leading to the development of electromagnetic cascades and reprocessing to lower energies. In the scenario of low- E_{\max} and mixed-composition cosmic-ray sources only, most of the gamma-ray signal is expected at GeV-PeV energies since the CR energies are insufficient for large interaction cross-sections with CMB photons. In this energy range (Fig. 3, top), the predicted gamma-ray flux associated with the PP protons in our model is at a similar level to the flux expected from the mixed cosmic rays. Depending on the exact choice of source parameters, the combined gamma-ray flux of both

populations can saturate the upper limit imposed by the re-scaled³ Fermi-LAT flux at ~ 700 GeV, however, the tension is not statistically significant. Most of the gamma-ray flux at $E_\gamma \gtrsim 100$ GeV is produced by the mixed-composition cosmic rays. At lower energies, the cosmogenic gamma rays are safely below the observed diffuse background flux.

The situation is more promising at ultra-high energies where the signal from the ordinary, mixed cosmic rays is expected to be very small. By construction, the protons injected at the PP sources have typical energies $E_\gamma > 10^{18}$ eV and consequently large cross-sections for photo-pion production on the abundant CMB photons. The predicted UHE gamma-ray flux from the protons is therefore orders of magnitude above the flux produced by the mixed cosmic rays (Fig. 3, bottom). It correlates inversely with the PP spectral index – harder injection spectra result in more cosmogenic UHE photons. As indicated previously, hard injection spectra generally require strongly positive redshift evolutions to soften the observed spectrum. Present limits by Auger and TA are not constraining, even in the most optimistic scenario within 3σ uncertainties, however, the difference is not more than a factor of a few and it is clear that future detectors – such as GRAND200k and AugerPrime – will provide strong constraints for the viable PP spectral index and redshift evolution.

The expected flux of cosmogenic neutrinos (Fig. 4) is not well constrained by the cosmic-ray fit alone and can vary by approx. a factor of 1000 within the 99.7% confidence interval. In the most pessimistic case, when the redshift evolution of the proton sources is strongly negative, the neutrino flux produced by PP protons is subdominant to the neutrinos from the default CR population at all energies $E_\nu \lesssim 1$ EeV and the UHE flux is small. On the other hand,

³ Following Alves Batista et al. (2019), we re-scale the isotropic gamma-ray background reported by Fermi-LAT (Ackermann et al. 2015) by a conservative factor of $\times 0.4$ to account for the contribution from unresolved point sources which was estimated to be $\approx 68^{+9}_{-8}\%$ by Lisanti et al. (2016).

Table 1. Best-fit parameters for the single- and two-population source models with EPOS-LHC used as the hadronic-interaction model describing air-shower development. The 1σ uncertainties include the penalty factor for the total best-fit quality proposed in [Rosenfeld \(1975\)](#). The “ISC” scenario is the benchmark model with only a single population of sources injecting mixed-composition cosmic rays. “Population 1” refers to the baseline source class that injects a mixed cosmic-ray flux of protons to iron, and “Population 2” denotes pure-proton sources. The best fit of UHECR spectrum and composition is given in the “CR” column, and the best fit after including neutrino and gamma-ray limits in the “CR + MM” columns. For the 2SC-uhecr model, the cosmic-ray best fit is compatible with existing multimessenger limits. Confidence intervals that extend to the edges of the sampled parameter range are indicated by an asterisk.

Model	ISC	2SC-dip CR	CR + MM	2SC-uhecr CR + MM
Population 1				
R_{\max} [EV]	$1.25^{+0.23}_{-0.19}$	$1.5^{+0.5}_{-0.4}$	$1.5^{+0.5}_{-0.4}$	$1.5^{+0.5}_{-0.4}$
γ	$-2.5^{+1.0}_{-0}$	$-1.20^{+0.22}_{-0.22}$	$-1.41^{+0.44}_{-0.22}$	$-1.41^{+0.22}_{-0.22}$
m	$1.9^{+0.6}_{-4.1}$	-2^{+2}_{-2}	-1^{+1}_{-3}	1^{+1}_{-2}
L_0 [$10^{44} \frac{\text{erg}}{\text{Mpc}^3 \text{ yr}}$]	$5.6^{+1.0}_{-3.4}$	$2.0^{+1.0}_{-0.5}$	$2.5^{+0.6}_{-1.0}$	$3.77^{+0.06}_{-1.39}$
f_p^R [%]	$6.6^{+15.4}_{-6.6}$	$\approx 0^{+6.5}_{-0}$	$\approx 0^{+8.6}_{-0}$	$\approx 0^{+7.2}_{-0}$
f_{He}^R [%]	$48.1^{+7.6}_{-2.8}$	$68.5^{+3.9}_{-7.3}$	$66.9^{+4.6}_{-4.8}$	$70.2^{+4.1}_{-4.4}$
f_N^R [%]	$40.1^{+4.9}_{-16.8}$	$26.6^{+6.6}_{-3.5}$	$28.0^{+4.5}_{-5.3}$	$23.6^{+3.0}_{-4.8}$
f_{Si}^R [%]	$4.8^{+0.7}_{-1.5}$	$4.5^{+0.5}_{-0.5}$	$4.8^{+0.3}_{-0.9}$	$5.8^{+0.6}_{-1.5}$
f_{Fe}^R [%]	$0.45^{+0.06}_{-0.17}$	$0.38^{+0.10}_{-0.09}$	$0.33^{+0.10}_{-0.05}$	$0.42^{+0.07}_{-0.08}$
Population 2				
E_{\max}^{PP} [EeV]		10^5 (fix)	10^5 (fix)	10 (fix)
γ^{PP}		$2.5^{+0.3}_{-0.3}$	$2.5^{+0.3}_{-0.3}$	$-0.25^{+0.50}_{-0.75}$
m^{PP}		6^{+0*}_{-10}	4^{+1}_{-10*}	-3^{+9*}_{-3*}
L_0^{PP} [$10^{44} \frac{\text{erg}}{\text{Mpc}^3 \text{ yr}}$]		$4.5^{+1.6}_{-4.0}$	$1.8^{+0.6}_{-1.4}$	$0.12^{+1.88}_{-0.06}$
$f^{\text{PP}}(20 \text{ EeV})$ [%]		$7.9^{+0}_{-0.9}$	$7.0^{+0.8}_{-0.5}$	$14.2^{+1.2}_{-0.5}$
χ^2/dof	101.0/29	73.4/26	74.4/26	58.0/26

for strong redshift evolutions, the expected neutrino flux saturates the flux observed by IceCube in the few-PeV energy range and exceeds significantly the limits above 10 PeV and at UHE. This includes the source configuration corresponding to the best UHECR spectrum and composition fit. By requiring that the neutrino limits are not violated ($\Delta\chi^2_\nu < 4$) we can constrain the properties of the proton sources to

$$\gamma^{\text{PP}} \gtrsim 1.6, \quad m^{\text{PP}} \lesssim 4, \quad \text{and} \quad L_0^{\text{PP}} \lesssim 10^{44.5} \frac{\text{erg}}{\text{Mpc}^3 \text{ yr}}. \quad (6)$$

Irrespective of the total level, the predicted neutrino flux exhibits a characteristic double-bump profile, with the first peak at $E_\nu \approx 5 \text{ PeV}$ from photo-pion production of the cosmic-ray protons on the extragalactic background light, and the second peak at $E_\nu \approx 1 \text{ EeV}$ from photo-pion production on the less energetic, but more abundant, CMB photons. Due to the soft spectrum of the UHE protons, both peaks are present at the same time and the UHE neutrino limits can be used to constrain the contribution of this cosmogenic neutrino flux to the observed IceCube HESE flux at 1.3 PeV to $f_{\text{HESE}}^{\text{PP}} \lesssim 20\%$.

4.2 2SC-uhecr

In the “UHECR best fit” model, the maximum proton energy is below the required level for photo-pion production with the bulk of CMB photons and the expected multimessenger signal is low. UHE

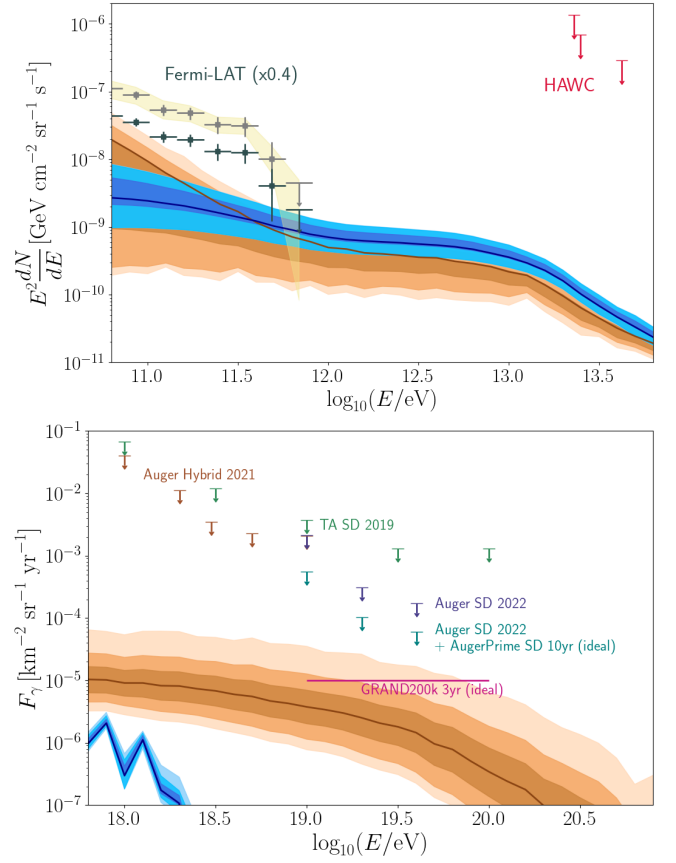


Figure 3. Predicted cosmogenic gamma-ray signal for the “proton-dip” model (2SC-dip), with Epos-LHC as hadronic interaction model, in the GeV–TeV (top) and EeV (bottom) energy range. The photon flux for each source class corresponding to the UHECR best fit (Tab. 1, 2nd and 4th column) is indicated by a solid line. The 1, 2, 3σ contours, under the condition that $\Delta\chi^2_\gamma < 4$, are indicated by brown bands in decreasing intensity for the contribution from the additional protonic UHECRs, and by blue bands for the neutrino flux from the regular, mixed cosmic rays. These intervals do not include the best-fit penalty factor of [Rosenfeld \(1975\)](#). Observations include the Fermi-LAT ([Ackermann et al. 2015](#)) and HAWC ([Albert et al. 2022](#)) diffuse gamma-ray background in the GeV–PeV range, the 95% upper limits at UHE of Auger ([Savina 2021; Abreu et al. 2022](#)) and TA ([Abbasi et al. 2019](#)), the optimistic 3-year sensitivity of the planned GRAND200k ([Álvarez-Muñiz et al. 2020](#)), and a combination of the latest Auger SD limit with the projected AugerPrime exposure for 10 years of observations under the assumption of 100% photon selection efficiency and zero background.

gamma rays are at least three orders of magnitude below existing limits and at GeV–TeV energies, the contribution is subdominant compared to the cosmogenic photons from the MIX cosmic rays. The total contribution to the Fermi-LAT IGRB is $< 50\%$ even in the most optimistic scenario, although the upper limit in the highest energy bin is approximately saturated.

While the neutrino signal of the UHE protons at the best fit is subdominant to the neutrinos from the mixed-composition cosmic rays, the shape of the neutrino spectrum is of particular interest. Unlike for the 2SC-dip model, few protons are present at lower energies and the low-energy peak originating from interactions with EBL photons is therefore absent. Only the peak from photo-pion production on the CMB remains. In this scenario, the observed IceCube neutrino flux at PeV energies and below, and the possible UHE neutrino flux are

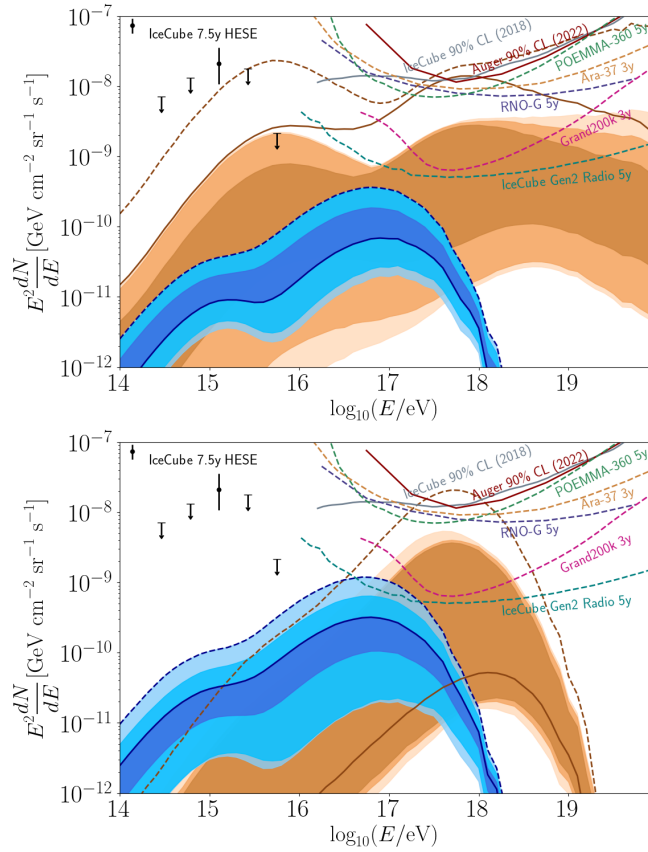


Figure 4. Same as Fig. 3 but for the predicted cosmogenic neutrinos in the 2SC-dip (top) and 2SC-uhcr model (bottom). The maximum allowed flux within 3σ of the best CR fit but without including the multimessenger penalty is shown as a dashed line of the respective colour. The IceCube HESE flux (Abbasi et al. 2021), upper limits from IceCube (Aartsen et al. 2018) and Auger (Aab et al. 2019; Pedreira 2021), and predicted sensitivities of planned detectors (Aartsen et al. 2019; Álvarez-Muñiz et al. 2020; Allison et al. 2016; Cummings et al. 2021) are shown as a reference.

decoupled. It is possible, for strongly positive redshift evolutions of the proton sources, to produce a large neutrino flux at UHE with a negligible contribution to the IceCube HESE flux. Redshift evolutions stronger than $m^{\text{PP}} \approx 4$ can be excluded by the current UHE neutrino limits of IceCube and Auger.

5 EXOTIC FLUX RECOVERY SCENARIO (2SC-REC)

A combination of the 2SC-dip and 2SC-uhcr models is provided by a proton source population with large maximum energy, $E_{\text{max}}^{\text{PP}} = 10^5$ EeV, as in the “proton-dip” model, and hard injection spectrum, $\gamma^{\text{PP}} = 1$, similar to the “UHECR” model. The quality of the UHECR fit (Tab. 2) is the worst out of all the three models and approaches the baseline single-source-class model. Compared to the dip model, the potential for fit improvement is limited since the protons contribute only at the highest energies, while the position of the observed proton peak is at too-high energies to provide an improvement of similar magnitude as in the 2SC-uhcr model. However, an interesting feature in the form of a “flux recovery” at trans-GZK energies can be observed (Fig. 5). We refer to this third model as the “recovery” or 2SC-rec model.

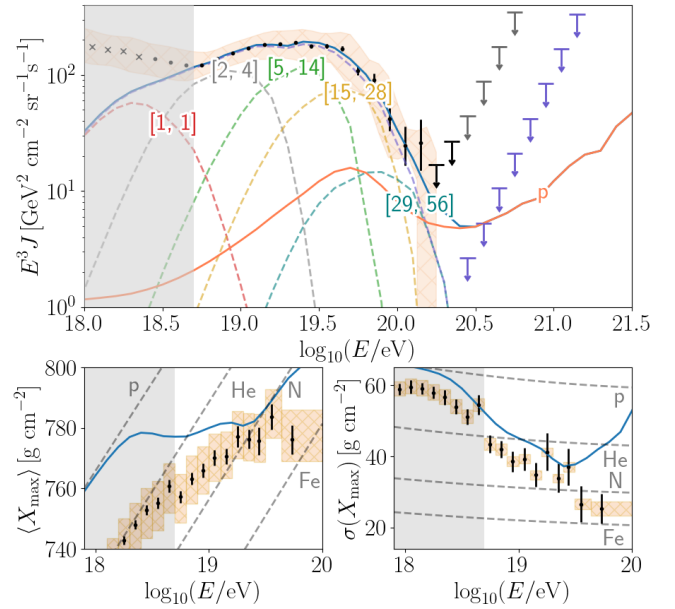


Figure 5. Same as Fig. 1 but for the “flux recovery” 2SC-rec scenario. Auger 90% upper limits above $10^{20.4}$ eV were derived assuming an energy-independent exposure of $60\,400\text{ km}^2\text{ yr sr}$ (Aab et al. 2020). Expected 90% upper limits for GCOS (40k) after 10 years of operation ($\epsilon \sim 10^6\text{ km}^2\text{ yr sr}$ (Coleman et al. 2023)) are shown in purple.

A recovery is only possible if the nearest source(s) is(are) located within the GZK volume at no more than ~ 20 Mpc (e.g. Gaisser et al. 2016) as otherwise, the GZK cutoff provides a natural suppression of the observable flux above $\sim 10^{19.7}$ eV. Such a spectral recovery is not necessarily connected to a large UHE neutrino signal. In addition to a high $E_{\text{max}}^{\text{PP}}$ and hard proton source spectra, the latter also requires strong redshift evolution of the source emissivity which is not a pre-requisite for a CR flux recovery. However, the observation of neutrinos with energy above 10^{19} eV by future extremely-UHE neutrino detectors such as PUEO (Abarr et al. 2021) would provide a strong hint for the existence of a sizeable UHECR flux recovery beyond the GZK cutoff.

We have noted in Sec. 4 for large $E_{\text{max}}^{\text{PP}}$ that hard proton source spectra are excluded by existing neutrino limits, under the condition that only source configurations within 3σ of the best fit to the UHECR spectrum and composition under the 2SC-dip model are considered. If this limitation is lifted, such as for the 2SC-rec model, we can identify scenarios where the predicted neutrino flux is sufficiently below existing limits, i.e. $\Delta\chi^2_{\nu} < 4$. This constrains the redshift evolution of the proton sources to $m^{\text{PP}} \lesssim 3$ ($\lesssim 2$ if gamma-ray limits are included).

In contrast to the 2SC-dip model, the combination of hard injection spectrum, high maximum proton energy and uniform source distribution with minimum distance $z_{\text{min}} = 10^{-3}$, results in an increased flux of cosmogenic UHE gamma rays. We find that for spectral indices harder than $\gamma^{\text{PP}} \lesssim 1$ all possible realisations of the source model are excluded by the existing Auger UHE photon limits (Savina 2021; Abreu et al. 2022). We conclude that the joint consideration of neutrino and UHE gamma-ray limits severely constrains the allowed proton injection spectrum and, by extension, the maximum allowed flux recovery from this second source population above the GZK cutoff. This motivates our choice of $\gamma^{\text{PP}} = 1$ as benchmark spectral index for the 2SC-rec model. The spectrum and composition corre-

Table 2. Same as Tab. 1 but for the extreme 2SC-recovery model. The best-fit parameters of the mixed-composition sources are given for the CR-only fit, but the preferred values for the CR+MM scenario are compatible within quoted uncertainties.

Population	MIX	f_A^R [%]	Pure-Proton	
			CR	CR + MM
R_{\max} [EV]	$1.4^{+1.0}_{-0.6}$	$10.5^{+7.6}_{-10.2}$	10^5 (fix)	10^5 (fix)
γ	$-1.7^{+0.4}_{-0.4}$	$55.7^{+4.5}_{-3.6}$	1 (fix)	1 (fix)
m	0^{+1}_{-1}	$29.3^{+4.8}_{-3.4}$	6^{+0*}_{-2}	2^{+1}_{-4}
L_0 [$10^{44} \frac{\text{erg}}{\text{Mpc}^3 \text{ yr}}$]	$3.3^{+0.8}_{-0.6}$	$4.3^{+1.0}_{-0.7}$	$12.0^{+1.7}_{-8.1}$	$1.5^{+0.6}_{-1.1}$
		$0.22^{+0.01}_{-0.02}$		
$f^{\text{PP}}(20 \text{ EeV})$ [%]			2.6^{+0}_{-0}	$1.46^{+0.06}_{-0.20}$
χ^2/dof			87.3/27	91.9/27

sponding to the maximum recovery allowed by the cosmic-ray fit and multimessenger constraints are shown in Fig. 5. The preferred source parameters stay unchanged except for the PP redshift evolution and luminosity density. Finally, we comment that the projected sensitivity of the proposed *Global Cosmic Ray Observatory* (GCOS) (Coleman et al. 2023) would place strong constraints on the allowed UHE flux recovery.

6 DISCUSSION

A similar conclusion in terms of the allowed UHE proton fraction for EPOS-LHC versus SIBYLL2.3C was reached in a recent paper by Muzio et al. (2023). The best fit obtained in this study is qualitatively similar to our 2SC-uhecr model with inverted proton injection spectra and low maximum energies. Their reported, best-fit observed proton fraction of the integral cosmic-ray flux above 30 EeV for typical astrophysical source evolutions is 5 – 10% and 2 – 3% for EPOS-LHC and SIBYLL2.3C respectively. These values are approximately compatible with our preferred integral fractions, $F^{\text{P}}(\geq 30 \text{ EeV}) = 10.2^{+1.4}_{-1.5}\%$ / $3.1^{+2.6}_{-0.9}\%$. A direct comparison is difficult, however, since the authors assumed a mono-elemental injection of Silicon-like nuclei as the MIX sources and also included in-source photo-hadronic interactions, and the predicted cosmic-ray flux at Earth is not provided.

A solution to the two-population model with source parameters similar to our 2SC-dip best fit was found in Das et al. (2021). However, the reported best-fit proton fraction at $E_{\text{ref}} = 20 \text{ EeV}$ is approx. 20 – 25% – a contribution that we found to be in strong tension with the observed UHECR composition, in particular the variance of shower maxima. The authors do not find the best fit of the UHECR spectrum and composition that we identify in our 2SC-uhecr model since they only consider soft spectral indices of the proton sources, $\gamma^{\text{PP}} \geq 2.2$, and no mention is made of a possible flux recovery beyond the GZK cutoff.

Important information about the potential sources of the UHE pure-proton flux can be gained from the total emissivity L_0^{PP} (luminosity density) required by the UHECR fit. Although the cosmic-ray emissivity of astrophysical objects is generally not known, other observable properties such as gamma-ray and X-ray emissivities can be used for relative calibration. For a summary of population emissivities see Murase & Fukugita (2019).

Assuming equipartition of the available energy budget into gamma rays / X-rays and cosmic rays, we observe that all typically considered source classes (gamma-ray bursts, tidal disruption events, starburst

galaxies, active galactic nuclei, BL Lacertae, flat-spectrum radio quasars, and radio galaxies) can satisfy the emissivity required of the pure-proton sources in the 2SC-uhecr and 2SC-dip models, although gamma-ray bursts and tidal disruption events are marginally challenged in the latter scenario.

For the extreme 2SC-recovery model, only the entire AGN population and the population of all BL Lacs can easily meet the required emissivity. GRBs and TDEs, in contrast, are excluded unless their cosmic-ray emissivity exceeds the observed gamma-ray emissivity by at least a factor of ten. FSRQs and radio galaxies sit close to the minimum luminosity density required by the cosmic-ray fit.

Given the hard spectrum and high maximum energy, it might be challenging that the UHE proton flux predicted by the 2SC-rec model is produced by astrophysical accelerators. An alternative explanation for the spectrum could be provided by the decay of hypothetical super-heavy dark matter (SHDM) with masses up to the Planck mass (Berezinsky et al. 1997; Kuzmin & Rubakov 1998; Sigl et al. 1999; Bhattacharjee & Sigl 2000; Ellis et al. 2006; Kalashev et al. 2009; Aloisio et al. 2015; Supanitsky & Medina-Tanco 2019). These heavy particles can be produced gravitationally during the early stages of the Universe, e.g. as part of the reheating epoch from a hypothesised, decaying inflaton field, or from coherent oscillations of this field before the inflation phase (Kofman et al. 1994; Felder et al. 1999; Chung et al. 1999). If they never reached thermal equilibrium after production and the lifetime is larger than the age of the Universe then these heavy relics can provide a possible explanation for observed DM densities (Aloisio et al. 2015).

Similar to the original proton-dip model (Berezinsky & Grigor'eva 1988), “top-down” scenarios of decaying SHDM are disfavoured as the single origin of the observed UHECR flux (Aab et al. 2017a; Rautenberg 2021), and it was shown that decaying SHDM cannot explain the detected high-energy IceCube neutrino events if a hadronic decay channel is considered (Kuznetsov 2017; Cohen et al. 2017; Kachelriess et al. 2018). Still, a subdominant contribution to the observed UHECR flux, and a possible flux recovery due to very hard decay spectra are not fully excluded. Crucially, existing upper limits on the post-GZK cosmic-ray flux provide only weak constraints on the allowed flux recovery, and UHE photon limits prove superior for $M_{\text{DM}} < 10^{14} \text{ GeV}$ (Supanitsky & Medina-Tanco 2019).

We do not investigate the SHDM scenario further, however, we wish to point out several key differences compared to our assumed source model. If the additional protons are produced in the decay of super-heavy dark matter, a substantial anisotropy in arrival directions and extremely local production of the observed UHECRs should be expected since the signal is predicted to be dominated by dark matter in the Milky Way with a particular clustering around the Galactic centre (Abreu et al. 2023). This is in sharp contrast to our proposed continuous distribution of sources in redshift up to $z_{\text{max}} = 4$ and minimum source distance of $\sim 4 \text{ Mpc}$. Consequently, in the SHDM scenario, the expected flux of cosmogenic neutrinos and low-energy gamma rays is severely reduced. In addition, we only consider the cosmogenic production of neutrinos and gamma rays while in the SHDM model the multimessenger signal is likely dominated by production during the decay of the dark matter.

7 SUMMARY AND CONCLUSIONS

In this work, we have investigated the possible existence, and allowed parameter space, for an additional, proton-dominated component of UHECRs, produced by an independent astrophysical source population. We have presented the maximum contribution of such a

population to the UHECR flux at Earth, taking into account the fit to the UHECR spectrum and composition-sensitive observables. In addition, we have derived predictions for the spectral shape and redshift evolution of the independent UHE-proton population model as well as the expected secondary neutrino and photon fluxes produced by UHECR interactions and their detectability.

This analysis was performed for two distinct choices of the maximum proton energy. For sources with maximum energy far beyond the GZK limit (2SC-dip model), the proton spectrum at Earth reproduces the predictions of the classic “proton-dip” model (Berezinsky & Grigor’eva 1988), albeit with the proton flux subdominant to the contribution of the principal, mixed-composition cosmic rays. If instead maximum energies below $10^{19.7}$ eV are assumed (2SC-uhecr model), the cosmic-ray fit is improved by $\Delta\chi^2 \approx -15$ but the source spectrum must be hard and the associated multimessenger signature is generally small. In both scenarios, the redshift evolution of the proton sources cannot be constrained by the cosmic-ray fit alone.

We find that the maximum proton contribution to the observed, diffuse UHECR flux depends strongly on the choice of hadronic interaction model for the interpretation of the extensive air showers, and on the maximum proton energy. With SIBYLL2.3c a proton fraction of $\lesssim 1\%$ is expected at 20 EeV in the 2SC-dip model and the improvement over the baseline model is negligible. Under the 2SC-uhecr model, a contribution of 2–5% is predicted with a 1.1σ significance fit improvement. Assuming Epos-LHC instead, for the 2SC-dip model, approximately 8% of the UHECR flux is expected to be protons, with the contribution approximately constant over the entire energy range above the ankle. For the 2SC-uhecr model, where $E_{\text{max}}^p = 10$ EV, the contribution to the observed UHECR flux peaks around $E_{\text{ref}} \approx 20$ EeV at up to 15%, but the relative proton fraction decreases rapidly for energies away from the peak and the source spectra are required to be hard. The improvement of the two-population model over the baseline single-population scenario is 2.2σ (2SC-dip) and 3.7σ (2SC-uhecr).

We demonstrated that for our fiducial high- E_{max}^p model a distinguishing feature of the independent UHE proton component is a soft spectral index (2.5 ± 0.3), which can be tested by AugerPrime or other facilities with event-by-event mass determination capabilities. In addition, the cosmogenic neutrino and UHE photon fluxes produced by this component are substantial and dominate over those from the mixed-composition population. Current neutrino upper limits from IceCube and Auger already weakly constrain the available parameter space for the proton population from the fit to the UHECR data alone.

Finally, as an “exotic” scenario, we have considered proton sources with high maximum energy $E_{\text{max}}^p \gg 10^{20}$ eV and hard spectral index. We find that existing limits on the neutrino and UHE gamma-ray flux constrain the proton spectral index to $\gamma^p \gtrsim 1$ and therefore provide an upper limit on the possible cosmic ray flux beyond the GZK cutoff. However, a significant recovery is still allowed.

ACKNOWLEDGMENTS

We thank Björn Eichmann, Michael Kachelriess, Marco Muzio, Pavlo Plotko, and Michael Unger for useful discussions.

DATA AVAILABILITY

No new observational data was generated as part of this study. The cosmic-ray, gamma-ray and neutrino propagation was simulated with

the CRPROP 3 software package (Alves Batista et al. 2016, 2022), which is publicly available from crpropa.desy.de.

REFERENCES

- Aab A., et al., 2017a, *JCAP*, 04, 009
Aab A., et al., 2017b, *JCAP*, 04, 038
Aab A., et al., 2017c, *JCAP*, 04, 038
Aab A., et al., 2017d, *Phys. Rev. D*, 96, 122003
Aab A., et al., 2019, *JCAP*, 10, 022
Aab A., et al., 2020, *Phys. Rev. D*, 102, 062005
Aartsen M. G., et al., 2018, *Phys. Rev. D*, 98, 062003
Aartsen M. G., et al., 2019, Neutrino astronomy with the next generation IceCube Neutrino Observatory ([arXiv:1911.02561](https://arxiv.org/abs/1911.02561))
Abarr Q., et al., 2021, *JINST*, 16, P08035
Abbasi R. U., et al., 2019, *Astropart. Phys.*, 110, 8
Abbasi R., et al., 2021, *Phys. Rev. D*, 104, 022002
Abdul Halim A., et al., 2022
Abreu P., et al., 2021, *PoS, ICRC2021*, 311
Abreu P., et al., 2022
Abreu P., et al., 2023, *Phys. Rev. D*, 107, 042002
Ackermann M., et al., 2015, *Astrophys. J.*, 799, 86
Albert A., et al., 2022
Allison P., et al., 2016, *Phys. Rev. D*, 93, 082003
Aloisio R., Matarrese S., Olinto A. V., 2015, *JCAP*, 08, 024
Álvarez-Muñiz J., et al., 2020, *Sci. China Phys. Mech. Astron.*, 63, 219501
Alves Batista R., et al., 2016, *JCAP*, 05, 038
Alves Batista R., de Almeida R. M., Lago B., Kotera K., 2019, *JCAP*, 01, 002
Alves Batista R., et al., 2022, *JCAP*, 09, 035
Baker S., Cousins R. D., 1984, *Nucl. Instrum. Meth.*, 221, 437
Berezinsky V. S., Grigor’eva S. I., 1988, *Astron. Astrophys.*, 199, 1
Berezinsky V., Kachelriess M., Vilenkin A., 1997, *Phys. Rev. Lett.*, 79, 4302
Bhattacharjee P., Sigl G., 2000, *Phys. Rept.*, 327, 109
Chung D. J. H., Kolb E. W., Riotto A., 1999, *Phys. Rev. D*, 60, 063504
Cohen T., Murase K., Rodd N. L., Safdi B. R., Soreq Y., 2017, *Phys. Rev. Lett.*, 119, 021102
Coleman A., et al., 2023, *Astropart. Phys.*, 149, 102819
Cummings A. L., Aloisio R., Krizmanic J. F., 2021, *Phys. Rev. D*, 103, 043017
Das S., Razzaque S., Gupta N., 2021, *Eur. Phys. J. C*, 81, 59
Das S., Murase K., Fujii T., 2023
Ehlert D., Oikonomou F., Unger M., 2022
Ellis J. R., Mayes V. E., Nanopoulos D. V., 2006, *Phys. Rev. D*, 74, 115003
Fedynitch A., Riehn F., Engel R., Gaisser T. K., Stanev T., 2019, *Phys. Rev. D*, 100, 103018
Felder G. N., Kofman L., Linde A. D., 1999, *Phys. Rev. D*, 59, 123523
Gaisser T. K., Engel R., Resconi E., 2016, *Cosmic Rays and Particle Physics: 2nd Edition*. Cambridge University Press
Gilmore R. C., Somerville R. S., Primack J. R., Domínguez A., 2012, *Mon. Not. Roy. Astron. Soc.*, 422, 3189
Greisen K., 1966, *Phys. Rev. Lett.*, 16, 748
Heinze J., Boncioli D., Bustamante M., Winter W., 2016, *Astrophys. J.*, 825, 122
Heinze J., Fedynitch A., Boncioli D., Winter W., 2019, *Astrophys. J.*, 873, 88
Heinze J., Biehl D., Fedynitch A., Boncioli D., Rudolph A., Winter W., 2020, *Mon. Not. Roy. Astron. Soc.*, 498, 5990
Ishiwata K., Macias O., Ando S., Arimoto M., 2020, *JCAP*, 01, 003
Kachelriess M., Kalashev O. E., Kuznetsov M. Y., 2018, *Phys. Rev. D*, 98, 083016
Kalashev O. E., Rubtsov G. I., Troitsky S. V., 2009, *Phys. Rev. D*, 80, 103006
Kofman L., Linde A. D., Starobinsky A. A., 1994, *Phys. Rev. Lett.*, 73, 3195
Kuzmin V. A., Rubakov V. A., 1998, *Phys. Atom. Nucl.*, 61, 1028
Kuznetsov M. Y., 2017, *JETP Lett.*, 105, 561
Lisanti M., Mishra-Sharma S., Necib L., Safdi B. R., 2016, *Astrophys. J.*, 832, 117
Luce Q., Marafico S., Biteau J., Condorelli A., Deligny O., 2022, *Astrophys. J.*, 936, 62
Mollerach S., Roulet E., 2020, *Phys. Rev. D*, 101, 103024

Murase K., Fukugita M., 2019, *Phys. Rev. D*, 99, 063012
 Muzio M. S., Unger M., Farrar G. R., 2019, *Phys. Rev. D*, 100, 103008
 Muzio M. S., Unger M., Wissel S., 2023
 Pedreira F., 2021, *PoS*, ICRC2019, 979
 Peters B., 1961, *Il Nuovo Cimento*, 22, 800
 Pierog T., Karpenko I., Katzy J. M., Yatsenko E., Werner K., 2015, *Phys. Rev. C*, 92, 034906
 Plotko P., van Vliet A., Rodrigues X., Winter W., 2022
 Rautenberg J., 2021, *PoS*, ICRC2019, 398
 Rodrigues X., Heinze J., Palladino A., van Vliet A., Winter W., 2021, *Phys. Rev. Lett.*, 126, 191101
 Rosenfeld A. H., 1975, *Ann. Rev. Nucl. Part. Sci.*, 25, 555
 Savina P., 2021, *PoS*, ICRC2021, 373
 Sigl G., Lee S., Bhattacharjee P., Yoshida S., 1999, *Phys. Rev. D*, 59, 043504
 Supanitsky A. D., Medina-Tanco G., 2019, *JCAP*, 11, 036
 Todero Peixoto C. J., 2019, *PoS*, ICRC2019, 440
 Unger M., Farrar G. R., Anchordoqui L. A., 2015, *Phys. Rev. D*, 92, 123001
 van Vliet A., Alves Batista R., Hörandel J. R., 2019, *Phys. Rev. D*, 100, 021302
 Waxman E., 1995, *Phys. Rev. Lett.*, 75, 386
 Yushkov A., 2020, *PoS*, ICRC2019, 482
 Zatsepin G. T., Kuzmin V. A., 1966, *JETP Lett.*, 4, 78

APPENDIX A: TWO-POPULATION FIT WITH SIBYLL2.3C

We find that the level of additional protons at UHE compatible with observations critically depends on the considered hadronic interaction model. With SIBYLL2.3C, the maximum improvement in fit quality over the single-population model is marginal for the high- $E_{\text{max}}^{\text{PP}}$ 2SC-dip model, and reaches a significance of 1.1σ for the 2SC-uhcr scenario.

Best-fit PP contributions to the observed flux at 20 EeV are at a level of $1.1^{+0.1}_{-1.0}\%$ and $2.4^{+3.1}_{-0.2}\%$ respectively (Tab. A1). The cosmic-ray best fit for both scenarios is shown in Fig. A1.

The pronounced differences between the two models are related to the quality of the single-population fit, in particular the $\langle X_{\text{max}} \rangle$ fit. While with SIBYLL2.3C a good fit of all observables can be achieved, EPOS-LHC is not able to provide a good fit of the spectrum and $\langle X_{\text{max}} \rangle$ at the same time. Consequently, for the latter, there is more room for improvement of the fit by an additional CR component, whereas for the two-population model with SIBYLL2.3C the potential is limited.

Although the contribution to the observed UHECR flux is generally low with SIBYLL2.3C, in the 2SC-dip model the associated flux of cosmogenic neutrinos and UHE gamma-rays can still be dominant compared to the fluxes derived from the mixed-composition cosmic rays (Fig. A2). However, they do not constrain the allowed PP source parameters except for $L_0^{\text{PP}} \lesssim 10^{44.3} \text{ erg Mpc}^{-3} \text{ yr}^{-1}$.

APPENDIX B: PROTON SOURCE PARAMETER SPACE

Results of the source-parameter scan are shown in Fig. B1 as a 2D surface plot over the PP injected spectral index $\gamma_{\text{src}}^{\text{PP}}$ and redshift evolution m^{PP} for both the 2SC-dip and 2SC-uhcr models.

This paper has been typeset from a \LaTeX file prepared by the author.

Table A1. Same as Tab. 1 but for SIBYLL2.3C as hadronic interaction model. The 2SC-dip best fit is excluded by the neutrino limits at $\Delta\chi^2_\nu \approx 4$, however, compatibility is obtained for $m^{\text{PP}} = 6 \rightarrow 5$. For the 2SC-uhcr scenario, the CR best fit is again compatible with the multimessenger constraints.

Model	1SC	2SC-dip	2SC-uhcr
Population 1			
R_{max} [EV]	$1.7^{+0.9}_{-0.6}$	$1.7^{+0.9}_{-0.6}$	$2.0^{+0.7}_{-0.9}$
γ	$0.15^{+0.59}_{-0.29}$	$0.15^{+0.59}_{-0.29}$	$0.54^{+0.22}_{-0.87}$
m	-4^{+4}_{-1}	-3^{+3}_{-3*}	-6^{+2}_{-0*}
L_0 [$10^{44} \frac{\text{erg}}{\text{Mpc}^3 \text{ yr}}$]	$1.61^{+1.12}_{-0.12}$	$1.74^{+1.0}_{-0.4}$	$1.41^{+0.19}_{-0.12}$
f_p^R [%]	$\approx 0^{+0}_{-0}$	$\approx 0^{+0}_{-0}$	$\approx 0^{+0}_{-0}$
f_{He}^R [%]	$66.9^{+2.5}_{-13.2}$	$63.4^{+6.1}_{-10.9}$	$70.4^{+0.7}_{-7.2}$
f_N^R [%]	$28.5^{+11.3}_{-2.3}$	$31.8^{+9.3}_{-5.6}$	$25.3^{+8.7}_{-0.8}$
f_{Si}^R [%]	$3.5^{+1.5}_{-0.1}$	$3.5^{+1.4}_{-0.4}$	$3.2^{+0.2}_{-2.1}$
f_{Fe}^R [%]	$1.1^{+0.4}_{-0.1}$	$1.3^{+0.3}_{-0.3}$	$1.1^{+0.7}_{-0}$
Population 2			
$E_{\text{max}}^{\text{PP}}$ [EeV]		10^5 (fix)	10 (fix)
γ^{PP}		$1.9^{+1.1*}_{-3.4*}$	$-1.3^{+1.3}_{-0.3*}$
m^{PP}		$6.0^{+0*}_{-12.0*}$	-6^{+12*}_{-0*}
L_0^{PP} [$10^{44} \frac{\text{erg}}{\text{Mpc}^3 \text{ yr}}$]		$0.7^{+5.9}_{-0.7}$	$0.012^{+0.401}_{-0.001}$
$f^{\text{PP}}(20 \text{ EeV})$ [%]		$1.1^{+0.1}_{-1.0}$	$2.4^{+3.1}_{-0.2}$
χ^2/dof	59.7/29	58.3/26	52.2/26

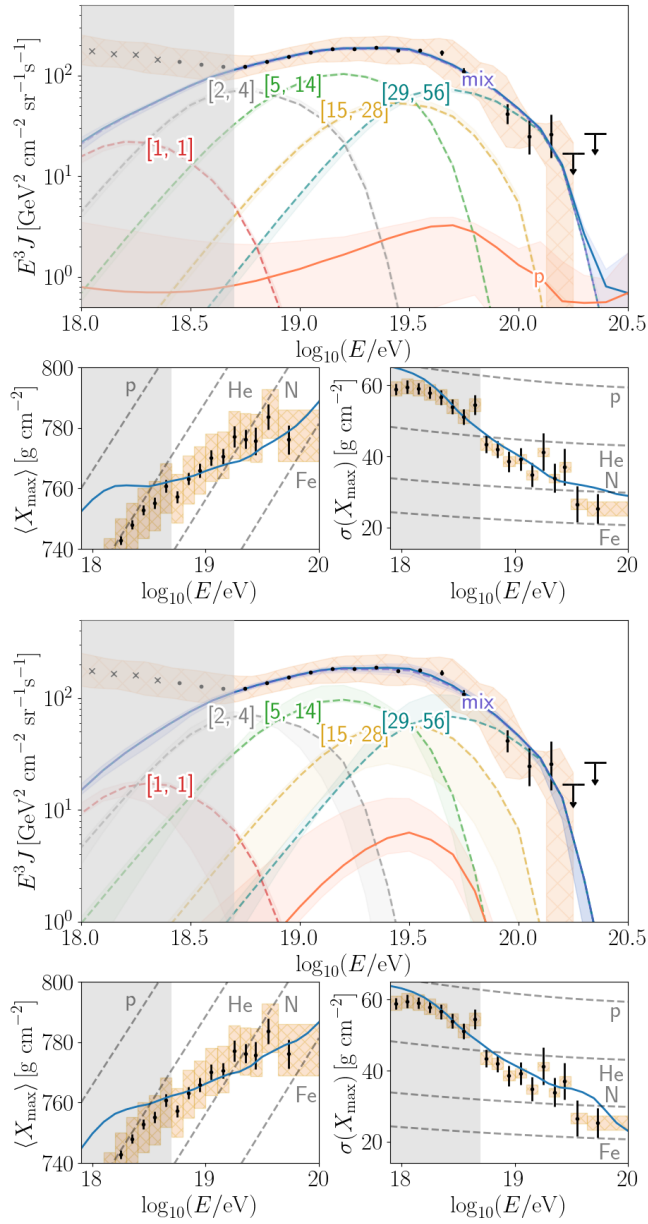


Figure A1. Same as Fig. 1 but with SIBYLL2.3c as hadronic interaction model. Top: “proton-dip” (2SC-dip). Bottom: “UHECR” best fit (2SC-uhedr). Best-fit parameters are listed in Tab. A1.

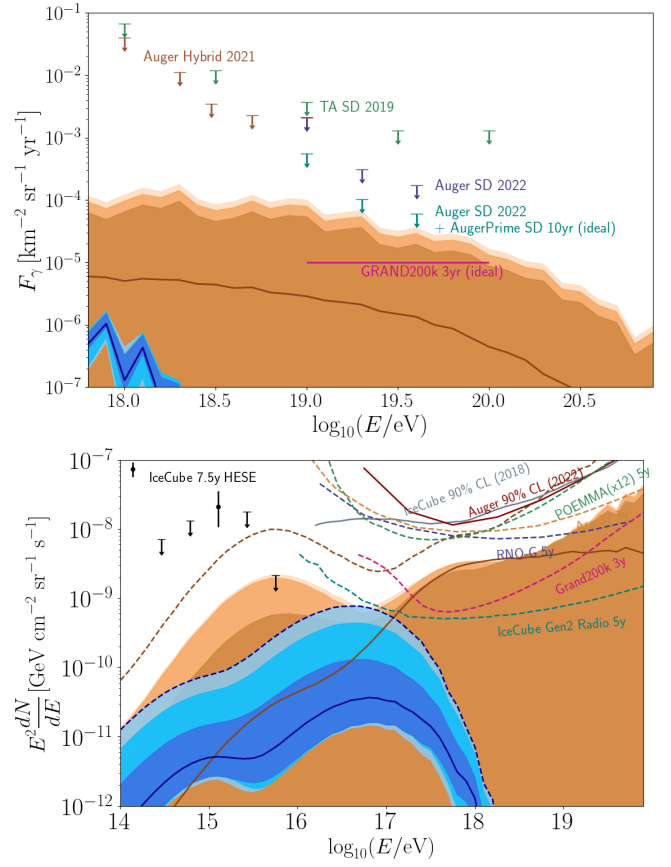


Figure A2. Same as Fig. 3 and Fig. 4 for the “proton-dip” model (2SC-dip) but with SIBYLL2.3c as hadronic interaction model. Top: UHE gamma rays. Bottom: neutrinos. The jagged upper limit of the UHE gamma-ray flux is a result of limited statistics in the numerical simulation.

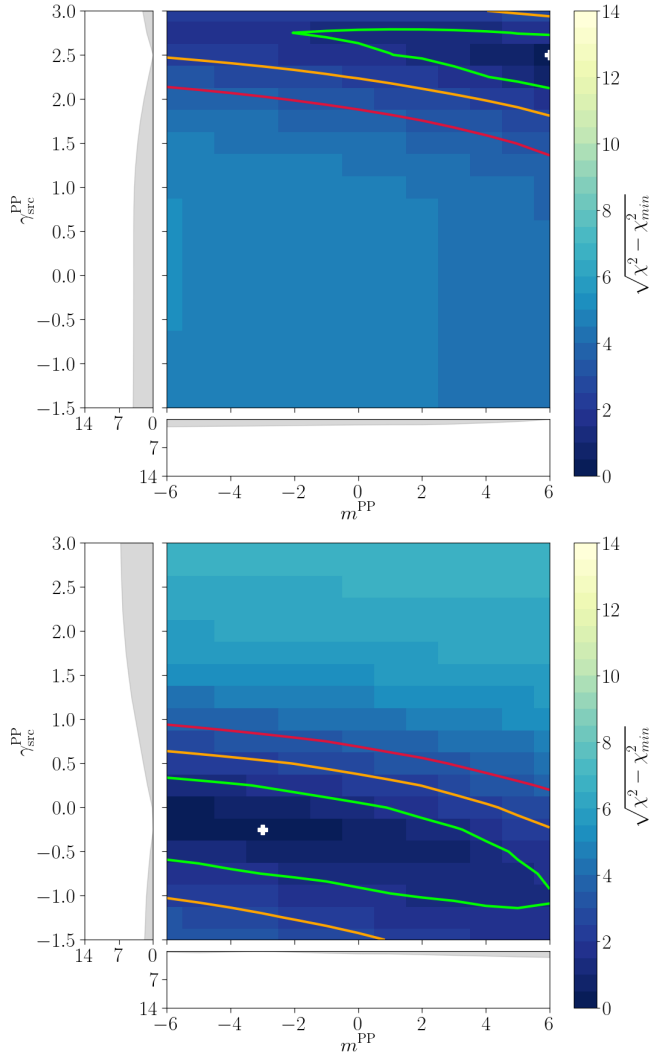


Figure B1. Fit quality for the 2SC-dip (top) and 2SC-uhecr (bottom) model, marginalised onto $\gamma_{\text{src}}^{\text{PP}} \times m^{\text{PP}}$ space. The best fit is marked with a white cross and contour lines indicate the one (green), two (orange) and three (red) sigma confidence intervals.